PCCP

Accepted Manuscript

ROYAL SOCIETY OF CHEMISTRY

www.rsc.org/pccp

Journal Name

RSCPublishing

ARTICLE

Lithium-Ion Diffusion Mechanisms in the Battery Anode Material $Li_{1+x}V_{1-x}O_2$

Cite this: DOI: 10.1039/xoxxoooooox

Pooja M. Panchmatia[a,c], A. Robert Armstrong[b], Peter G. Bruce[b], M. Saiful Islam*[a]

Received ooth January 2012,
Accepted ooth January 2012

DOI: 10.1039/xoxxoooooox

www.rsc.org/

Layered $Li_{1+x}V_{1-x}O_2$ has attracted recent interest as a potential low voltage and high energy density anode material for lithium-ion batteries. A greater understanding of the lithium-ion transport mechanisms is important in optimising such oxide anodes. Here, stoichiometric $LiVO_2$ and Li-rich $Li_{1.07}V_{0.93}O_2$ are investigated using atomistic modelling techniques. Lithium-ion migration is not found in $LiVO_2$, which has also previously shown to be resistant to lithium intercalation. Molecular dynamics simulations of lithiated non-stoichiometric $Li_{1.07+y}V_{0.93}O_2$ suggest cooperative interstitial Li^+ diffusion with favourable migration barriers and diffusion coefficients (D_{Li}), which are facilitated by the presence of lithium in the transition metal layers; such transport behaviour is important for high rate performance as a battery anode.

1. Introduction

The revolution in portable electronic devices has been powered by rechargeable lithium-ion batteries. Alternative electrode materials for new generations of lithium batteries are generating considerable research activity, particularly for large-scale applications (such as electric vehicles and grid storage).[1-9] Graphite is currently the dominant anode material in Li-ion batteries. Metal oxide anodes such as TiO_2(B) are attracting interest since they can offer twice the volumetric energy density of graphite.[10-12] However, the anode voltage for titanium oxides of ~1.6V vs Li+/Li compared to ~0.1V for graphite compromises the cell voltage and hence energy storage.

Recent studies have shown that Li can be intercalated into the layered oxide $Li_{1+x}V_{1-x}O_2$, at an unusually low voltage of ~0.1 V vs. Li^+/Li[13-20], with a theoretical volumetric capacity of 1,360 $mAhcm^{-3}$ compared to graphite at 790 $mAhcm^{-3}$. Previously we investigated the intercalation process for $Li_{1+x}V_{1-x}O_2$ and in particular the key role that non-stoichiometry or excess lithium ($x > 0$) plays in switching on intercalation.[16] Lithium does not intercalate into stoichiometric layered $LiVO_2$ (Fig 1). However, substituting a small of the V on the transition metal sites by Li (typically $Li_{1.07}V_{0.93}O_2$) is sufficient to promote a two-phase intercalation process at a potential of ~0.1V.

Other recent studies on this system[17] include an investigation of doping on the V site with Cr or Fe leading to improved rate capabilities and cyclability. A combination of solid state NMR, pair distribution function analysis and density functional theory calculations has provided further insights into the crystal and electronic structures of $Li_{1+x}V_{1-x}O_2$, indicating magnetically-induced distortions of the V sublattice to form trimers.[18]

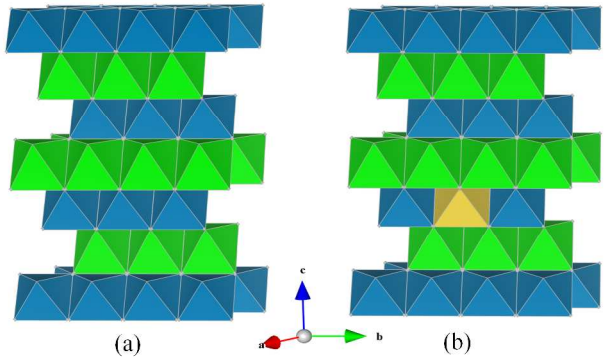

Figure 1. Schematic representation of the layered structures of (a) $LiVO_2$, and (b) $Li_{1.07}V_{0.93}O_2$. Key: LiO_6 octahedra (green); VO_6 octahedra (blue); Li on V site (yellow)

To fully understand the factors influencing the electrochemical behaviour of the $Li_{1+x}V_{1-x}O_2$ anode material it is clear that greater insight into the underlying lithium transport properties is needed at the atomic scale. Indeed, a major puzzle is what is the atomistic mechanism controlling lithium-ion diffusion in this new oxide anode? Such transport features are important factors for charge/discharge rates and high power,

but are often difficult to determine from experimental methods. Here, we extend our previous electrode work with a combination of energy minimization and molecular dynamics (MD) simulation techniques to probe, for the first time, the lithium-ion diffusion mechanisms in the vanadate material. In particular, the results comparing stoichiometric $LiVO_2$ and Li-rich $Li_{1.07}V_{0.93}O_2$ from long time-scale MD provide new insights into the mechanistic features of interstitial lithium-ion transport.

2. Methods

Atomistic modelling techniques are well suited to the investigation of defect and transport properties and have been applied successfully to a variety of studies on lithium battery materials.[21-26] In the present study, potentials-based energy minimization and molecular dynamics (MD) were employed.[25-27] The GULP code[28] was used for the interatomic potential refinement, and the Mott-Littleton[29] method was used to investigate the isolated point defects. The interactions between ions were represented in terms of a long-range Coulombic term plus an analytical function representing short-range repulsive and van der Waals forces. The empirically-derived potential parameters for Li-O, V-O and O-O were transferred from our previous successful study of the $LiVO_2$ system.[16] The Buckingham shell-model potentials used in this study are presented in Supplementary information, Table S1.

The MD technique consists of an explicit dynamical simulation of the ensemble of ions for which Newton's equations of motion are solved (and were carried out using the DLPOLY 2.20 code).[27] For this work two key structural compositions were compared: stoichiometric $LiVO_2$ and the lithiated non-stoichiometric $Li_{1.07+y}V_{0.93}O_2$ (where y=0.09). The $LiVO_2$ simulation box was constructed using a 10 x 10 x 2 P1 supercell consisting of 2,400 atoms. Our previous work showed that Li intercalation into the Li-rich $Li_{1.07}V_{0.93}O_2$ phase was energetically more favourable and that the Li interstitials preferred to go on a tetrahedral site adjacent to a Li on a vanadium site.[16] The initial $Li_{1.07+y}V_{0.93}O_2$ configuration contained 10% Li interstitial ions placed on these tetrahedral sites leading to a total of 2,454 atoms in the supercell. The charge-compensation for Li on the V sites and Li interstitials was delocalised across all the V ions to make the supercell charge neutral. More than three initial configurations of the lithiated lithium vanadium oxide were explored via full bulk optimisations; their energetic stabilities were compared and the lowest energy configuration was used for the subsequent MD simulations.

After initial equilibration (100,000 steps), MD simulations were performed with a 0.5 fs time step for long runs of 1.1 ns at a range of temperatures in the range 200 - 600K (Nóse – Hoover thermostat[27]) at intervals of 100K. The NPT ensemble was used to allow for any thermal expansion after which the NVT ensemble was employed for the full production runs of 1.1ns, which are important for good statistics. Such potentials-based MD techniques have been applied to other lithium battery materials[23,24] and to oxide-ion conductors for solid oxide fuel cells.[30] It is worth remarking that we are employing much larger supercells and an order of magnitude longer timescales than the majority of *ab initio* MD simulations.

Table 1. Comparison of experimental[16] and calculated structural parameters for $LiVO_2$ and $Li_{1.07}V_{0.93}O_2$. Elastic and dielectric properties have been presented in Supplementary information, Table S2.

(a)	$LiVO_2$ (R-3m)		
	Expt.	Calc.	Δ
a /Å	2.8377	2.8608	0.023
b /Å	2.8377	2.8608	0.023
c / Å	14.8230	14.5516	-0.271
α / β deg	90.0	90.0	0.0
γ /deg	120.0	120.0	0.0
Li – O / Å	2.102	2.103	0.001
V – O / Å	2.004	2.058	0.054
O – O / Å	2.830	2.905	0.075
(b)	$Li_{1.07}V_{0.93}O_2$ (R-3m)		
	Expt.	Calc.	Δ
a /Å	2.8430	2.9370	0.094
b /Å	2.8430	2.8920	0.049
c / Å	14.7675	14.6355	-0.132
α / β deg	90.0	90.0	0.0
γ /deg	120.0	120.0	0.0
Li – O / Å	2.020	2.064	0.044
Li^{+}_{V} – O / Å	2.046	2.030	-0.016
V – O / Å	2.037	2.030	-0.007
O – O / Å	2.834	2.832	0.002

3. Results and Discussion

3.1 Structures and defect chemistry

The $LiVO_2$ and the $Li_{1.07}V_{0.93}O_2$ are both *ccp* structures (space group R-3m) with alternating LiO_6 and VO_6 layers shown schematically in figure 1; the lithium present in the transition metal layers in $Li_{1.07}V_{0.93}O_2$ is highlighted. The modelling study first attempted to reproduce the observed crystal structures. A comparison between the calculated unit cell parameters based on effective potentials and those of the experimental structure is given in Table 1. The calculated unit cell parameters deviate from experiment by at most 1.9%, and in most cases much less; the same is found for the Li-O and V-O bond lengths. This reproduction of the structures of both $LiVO_2$ and $Li_{1.07}V_{0.93}O_2$ compositions gives us confidence that the interatomic potential model can be used reliably in the defect and migration calculations. In Supplementary information, we have also listed the calculated elastic and dielectric constants for $LiVO_2$ and $Li_{1.07}V_{0.93}O_2$. Although there are no experimental data for the LiVO2 system for direct comparison, our calculated values are consistent

with observed and DFT values for similar layered oxides[31] including static dielectric constants for $LiCoO_2$.

A series of isolated point defect (vacancy and interstitial) energies were then calculated, and combined to give the relative energies of formation of the Li Frenkel defect. We also examined the Li/M "anti-site" pair defect, which involves the exchange of a V ion (radius 0.64 Å) with a Li ion (radius 0.76 Å); this type of defect is worth investigating since cation exchange effects have been observed in other layered oxide electrodes.[1,2]

Table 2 lists the formation energies of Li Frenkel or anti-site defects in the two compositions. The high unfavourable energies suggest that the inability to intercalate into stoichiometric $LiVO_2$ is not due to the presence of site-exchange disorder involving V ions in the alkali metal layers pinning them together; this result is in agreement with previous structural studies indicating that there is no V in the Li layers of $LiVO_2$. The site exchange energy in $Li_{1.07}V_{0.93}O_2$ is the most favourable, although the magnitude still suggests that intrinsic concentrations will not be significant. The calculated defect energies also suggest that intrinsic lithium vacancies and interstitials are unlikely to be found in stoichiometric $LiVO_2$.

Table 2. Formation energies of lithium Frenkel and anti-site defects. (The reaction equations can be found in the Supplementary information.)

Compound	Frenkel defect energy (eV)	Antisite defect ener (eV)
$LiVO_2$	3.58	3.44
$Li_{1.07}V_{0.93}O_2$	1.67	1.36

3.2 Li ion diffusion

Examination of the Li-ion transport properties of $Li_{1+x}V_{0.93}O_2$ is of vital importance when considering electrode kinetics. Of primary interest here is information on the atomistic mechanism of lithium-ion diffusion, which is difficult to probe purely by experimental methods. Molecular dynamics (MD) techniques are well suited to probing transport mechanisms directly especially cooperative or correlated ion motion. Here, MD calculations over long simulation time scales were carried out at temperatures more than covering typical battery operating temperatures for the two compositions for direct comparison: stoichiometric $LiVO_2$ and the lithiated non-stoichiometric $Li_{1.07+y}V_{0.93}O_2$ (y=0.09).

First, the mean squared displacements (MSDs), $\langle[r(t)]^2\rangle$, of lithium ions have been resolved and shown in Figure 2; the results clearly show that there is only significant lithium-ion diffusion in the Li-rich composition. For $LiVO_2$ the MSD of the Li-ions tends rapidly to a constant value and confirms that there is no ion diffusion in this stoichiometric composition.

The Li-ion diffusion coefficient (D_{Li}) can be derived from the MSD data given by $D = (1/6t)\langle[r(t)]^2\rangle$. We calculate a D_{Li} value of about 10^{-9} cm^2s^{-1} for $Li_{1.07+y}V_{0.93}O_2$ (y=0.09) at 300K. Although there are currently no measured diffusion data for direct comparison, the magnitude is comparable to other electrode materials; for example, graphite has lithium diffusivity of about 10^{-8} to 10^{-9} cm^2s^{-1},[32] and experimental diffusion coefficients of 10^{-8} to 10^{-11} cm^2s^{-1} have been reported[33] for Li+ diffusion in layered oxide cathodes such as $LiCoO_2$ and $Li(Ni,Mn,Co)O_2$.

An Arrhenius plot (lnD versus 1/T) for lithiated $Li_{1.16}V_{0.93}O_2$ is presented in Figure 3. Analysis of such data provides an estimate of the migration activation energy (E_{act}) using the standard Arrhenius relation:

$$D = A\exp(-E_{act}/kT) \quad (1)$$

A migration activation energy of 0.32 eV is derived, indicating high Li ion mobility in this Li-rich oxide anode, which is important for good rate capability. Despite the lack of Li ion conductivity data for direct comparison, our calculated migration energy is compatable with low activation energies for other layered oxides such as $Li_xCo_{0.95}Mg_{0.05}O_2$[34], Li_xCoO_2[26] and Li_xNiO_2[35], albeit for Li vacancy migration.

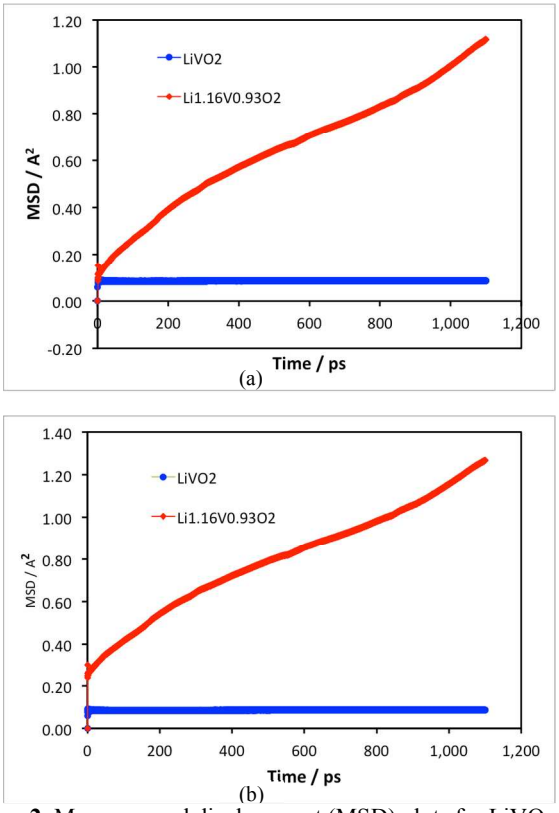

Figure 2. Mean squared displacement (MSD) plots for $LiVO_2$ (blue) and $Li_{1.07+y}V_{0.93}O_2$ (red) for 1.1 ns at (a) 400 K and (b) 500 K.

Scatter or density plots of the accumulated density of lithium ion trajectories over the simulated time scale enables useful visualization of the migration pathways and the lattice regions most frequently traversed by the mobile Li-ions. Figure 4a shows the starting configuration of the $Li_{1.07+y}V_{0.93}O_2$ (y=0.09) structure where the Li^+_V atoms are in the vanadium layers and the interstitial lithums are on tetrahedral sites. As shown previously,[16] substitution of Li for V on the octahedral

transition metal sites renders tetrahedral sites in the alkali metal layers energetically accessible by Li.

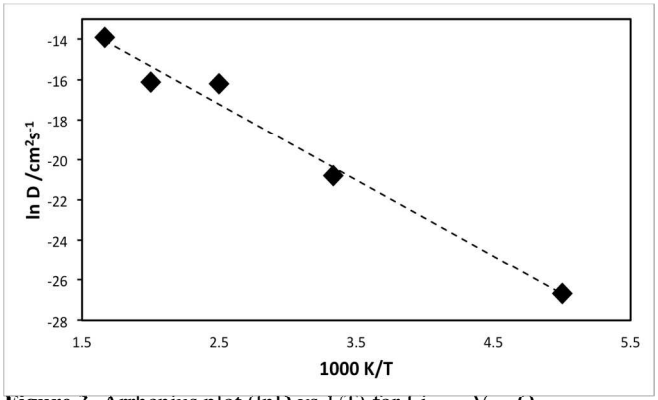

Figure 3. Arrhenius plot (lnD vs 1/T) for $Li_{1.07+y}V_{0.93}O_2$.

The lithium diffusion density plots and final configuration of ions in $Li_{1.07+y}V_{0.93}O_2$ (y=0.09) at the end of the MD simulation are shown in Figure 4b. The diffuse distribution and overlapping of different lithium positions indicate that numerous different lithium ions are moving between octahedral lattice and tetrahedral interstitial sites. These results show that long-range lithium-ion migration is highly anisotropic, restricted to within the lithium layers adjacent to vanadium layers that contain a small amount of lithium ions. Interestingly, there is also evidence of ion migration between adjacent layers *via* the lithium ions on the V sites. In contrast, the lithium layers that are not adjacent to Li on V sites, do not exhibit

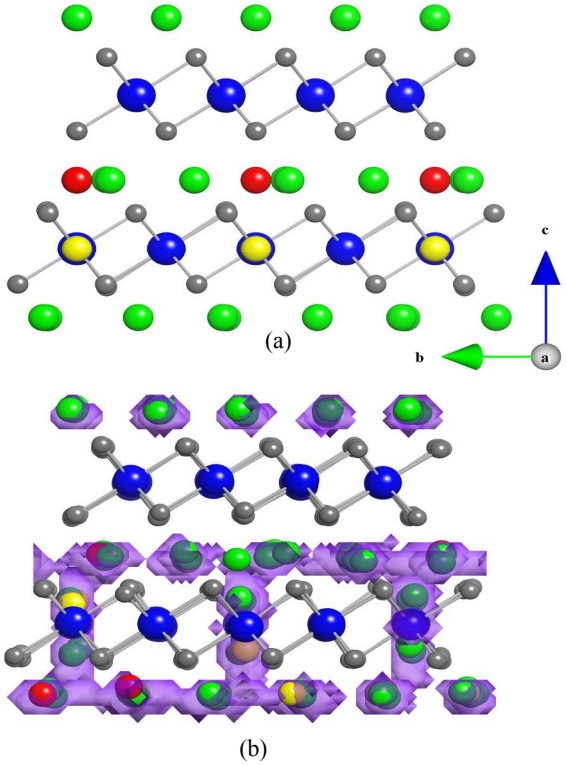

Figure 4. (a) Ion positions of the initial configuration of $Li_{1.07+y}V_{0.93}O_2$ (y=0.09) (b) MD density plot of mobile lithium ions (purple) overlayed on a snapshot of the final configuration after 1.1ns. Key: octahedral Li (green); octahedral V (blue); Li on V site (yellow); interstitial Li (red) ; O (grey).

diffusion within or across the layers. A key feature is that the Li-rich composition with Li on V sites plays a vital role in not only switching on the lithium intercalation process[16], but also in aiding facile lithium-ion diffusion.

A major thrust of fundamental transport studies has been the

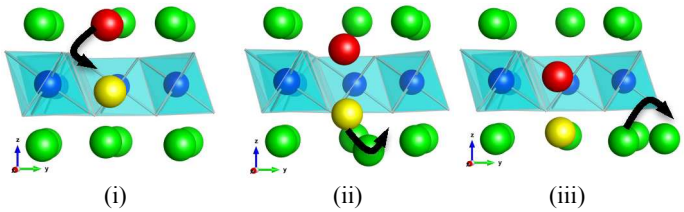

Figure 5. MD simulation snapshots of ion positions showing the knock-on like mechanism: the migrating interstitial Li^+ (red) displaces the Li in the V layer (yellow) into an adjacent interstitial position which in turn leads to further Li migration. The oxygen atoms have been omitted for clarity. Key: octahedral Li (green); octahedral V (blue)

examination of the atomistic mechanisms controlling bulk transport phenomena. Indeed, the unravelling of mechanistic detail at the microscopic level is a powerful feature of the MD technique. Figure 5 shows a series of snapshots of the lithium ions as they migrate within the alkali-ion layer and *via* the Li ions in the vanadium layers. This suggests that lithium-ion diffusion takes place by a cooperative interstitialcy or knock-on type mechanism in which the migrating interstitial Li-ion displaces the Li in the V layer into a neighbouring interstitial position in the alkali-metal layer. Such a cooperative type mechanism facilitates lithium-ion diffusion despite the lack of open conduction pathways. Similar cooperative mechanisms have been discussed in connection with lithium migration in $LiMgSO_4F$[24] and with interstitial oxide-ion conduction in electrolytes for solid oxide fuel cells,[30,31] but have not been widely elucidated in Li-rich layered oxides.

4. Conclusions

Atomic-scale mechanistic features of Li-ion transport in vanadium oxide anode materials have been investigated, revealing three main results.

First, the defect formation energies indicate that the inability to intercalate into stoichiometric $LiVO_2$ is not due to the presence of cation exchange disorder involving V ions in the lithium ion layers pinning them together, which is in agreement with structural studies. It is known that the Li-rich composition $Li_{1.07}V_{0.93}O_2$ with lithium on the vanadium layers switches on lithium intercalation.

Second, the MD simulations indicate facile Li^+ diffusion in the lithiated composition, $Li_{1.07+y}V_{0.93}O_2$, with a low activation barrier (0.32 eV) for interstitial Li^+ transport, and diffusion coefficients (D_{Li}) of ca. 10^{-9} cm^2s^{-1}; these values are consistent with other layered oxide electrodes and suggest favourable rate performance. Finally, long-range Li^+ diffusion is found to be highly anisotropic, largely restricted to within the lithium layers adjacent to vanadium layers that contain lithium ions. Interestingly, there is also evidence of interlayer diffusion *via*

the lithium ions on the vanadium sites, and involving a cooperative interstitial mechanism.

These results on transport mechanisms and electrode kinetics are valuable in developing strategies for optimizing this low voltage oxide anode.

Acknowledgements

We acknowledge EPSRC for funding (EP/H019596/1) and the Materials Chemistry consortium (EP/L000202/1) for access to high-end supercomputer resources. PMP would like to thank D. J. Cooke for useful discussions.

Notes and references

[a] Department of Chemistry, University of Bath, Bath BA2 7AY, U.K; m.s.islam@bath.ac.uk.
[b]School of Chemistry, University of St. Andrews, St. Andrews, Fife, U.K.
[c]Department of Chemical Sciences, University of Huddersfield, Huddersfield, U.K.

[1] J. B. Goodenough, *Chem. Mater.*, 2010, **22**, 587
[2] B. L. Ellis, K. T. Lee and L. F. Nazar, *Chem. Mater.*, 2010, **22**, 691.
[3] M. S. Whittingham, *MRS Bull.*, 2008, **33**, 411.
[4] M. Armand and J.-M. Tarascon, *Nature*, 2008, **451**, 652.
[5] P.G. Bruce, B. Scrosati, and J. M. Tarascon, *Angewandte Chem.-International Edition*, 2008, **47**, 2930; B. Scrosati, J. Hassoun and Y.-K. Sun, *Energy Environ. Sci.*, 2011, **4**, 3287.
[6] M. R. Palacín, *Chem. Soc. Rev.*, 2009, **38**, 2565.
[7] M. M. Thackeray, C. Wolverton and E. D. Isaacs, *Energy Environ. Sci.*, 2012, **4**, 7854.
[8] J. Liu, J.-G. Zhang , Z. Yang , J. P. Lemmon, C. Imhoff, G. L. Graff, L. Li, J. Hu , C. Wang, J. Xiao, G. Xia, V. V. Viswanathan, S. Baskaran, V. Sprenkle, X. Li, Y. Shao and B. Schwenzer, *Adv. Funct. Mater,* 2013, **23**, 929.
[9] N. S. Choi, J. S. Kim, R. Z. Yin and S. S. Kim, *Mater. Chem. Phys.*, 2009, **116**, 603.
[10] G. Zhu, Y-G Wang and Y-Y Xia, *Energy Environ. Sci.*, 2012, **5**, 6652.
[11] M.V. Reddy, G.V. Subba Rao, and B.V. R. Chowdari, *Chem. Rev.*, 2013, **113**, 5364.
[12] L. Ji, Z. Lin, M. Alcoutlabi and X. Zhang, *Energy Environ. Sci.*, 2011, **4**, 2682.
[13] J. H. Song, H. J. Park, K. J. Kim, Y. N. Jo, J – S. Kim, Y. U. Jeong and Y. J. Kim, *J. Power Sources*, 2010, **195**, 6157.
[14] S. –S. Kim, J. Kim, M. Koike and N. Kobayashi, 14th International Meeting on Lithium Batteries, Tianjin, Abstract #20 (2008).
[15] S–S. Kim, Y. Nitta, T. I. Nedoseykina, and J–C. Lee, US Patent Application US 2006/0088766 (2006).
[16] A.R. Armstrong, C. Lyness, P.M. Panchmatia, M.S. Islam, P.G. Bruce, *Nature Mater.*, 2011, **10,** 223.
[17] W-T, Kim, Y. U. Jeong, H. C. Choi, Y. J. Lee, Y. J. Kim, J. H. Song, *J. Power Sources*, 2013, **221**, 366.
[18] F. Pourpoint, X. Hua, D. S. Middlemiss, P. Adamson, D. Wang, P. G. Bruce, C. P. Grey, *Chem. Mater.*, 2012, **24**, 2880.
[19] J.Yi, J. Key, F. Wang, Y-G Wang, C. Wang, Y-Y Xia, *Electrochimica Acta,* 2013, **106**, 534; J.M. Gaudet and J.R. Dahn, *Can. J. Phys*., 2013, **91**, 444.
[20] Y. C. K. Chen-Wiegart, *Electrochem. Comm,* 2012, **21**, 58.
[21] C.A.J. Fisher and M.S. Islam, *J. Mater. Chem*. 2008, **18**, 1208; M. Schroeder, C. Eames, D. A. Tompsett, G. Lieser and M. S, Islam, *Phys. Chem. Chem. Phys*., 2013, **15**, 20473.
[22] M. S. Islam, D. J. Driscoll, C. A. J. Fisher, P. R. Slater, *Chem. Mater.*, 2005, **17**, 5085; G. R. Gardiner and M. S. Islam, *Chem. Mater.* 2010, **22**, 1242; N. Kuganathan and M.S. Islam, *Chem. Mater*., 2009, **21**, 5196.
[23] S. Lee and S.S. Park, *J. Phys. Chem*. C, 2012, **116**, 6484; C. Tealdi, C. Spreafico and P. Mustarelli, *J. Mater. Chem*., 2012**, 22**, 24870; S. Adams and R.P. Rao, *Solid State Ionics*, 2011, **184**, 57; M. Vijayakumar, S. Kerisit, K.M. Rosso, S.D. Burton, J.A. Sears, Z. Yang, G.L. Graff, J. Liu and J. Hu, *J. Power Sources*, 2011, **196**, 2211; S.E. Boulfelfel, G. Seifert and S. Leoni, *J. Mater. Chem*., 2011, **21**, 16365.
[24] M. Salanne, M. Marrocchelli, G. W. Watson, *J. Phys. Chem. C.*, 2012, **116**, 18618.
[25] C. R. A. Catlow, (ed) "Computer Modelling in Inorganic Crytallography", Academic Press, San Diego 1997.
[26] M.S. Islam and C. A. J. Fisher, *Chem. Soc. Rev*., 2014, **43**, 185.
[27] W. Smith, C. W. Yong and P. M. Rodger, *Mol. Simul.*, 2002, **28**, 385; S. Nóse, *J. Chem. Phys.,* 1984, **81**, 511; W. G. Hoover, *Phys. Rev. A*., 1985, **31**,1695.
[28 J. D. Gale, *J. Chem. Soc. Faraday Trans.*, 1997, **93**, 629.
[29] N. F. Mott and M. J. Littleton, *Trans. Faraday Soc.*, 1938, **34**, 485.
[30] C. Tealdi, P. Mustarelli, M. S. Islam, *Adv. Func. Mater*. 2010, **20**, 3874; E. Kendrick, J. Kendrick, K. S. Knight, M. S. Islam, P. R. Slater, *Nature Mater*. 2007, **6**, 871; P. M. Panchmatia, A. Orera, G. J. Rees, M. E. Smith, J. V. Hanna, P. R. Slater, M. S. Islam, *Angew. Chem. Int. Ed.,* 2011, **50**, 9328; A. Chroneos, D. Parfitt, J. A. Kilner, R. W. Grimes, *J. Mater. Chem.* 2010, **20**, 266.
[31] K. Hoang and M.D. Johannes, *J. Mater. Chem. A*, 2014, 2, 5224; F.X. Hart and J.B. Bates, *J. Appl. Phys.,* 1998, 83, 7560.
[32] K. Persson, V. A. Sethuraman, L. J. Hardwick, Y. Hinuma, Y-S Meng, A. van der Ven, V. Srinivasan, R. Kostecki, G. Ceder, *J. Phys. Chem. Lett.*, 2010, **1**, 1176; S. Bhattacharya, A. R. Riahi, A. T. Alpas, *Carbon* 2014, **67**, 597; D. R. Baker, M. W. Verbugge *J. Electrochem. Soc.* 2012, **159**, A1341; P. Maire, H. Kaiser, W. Scheifele, P. Novak *J. Electroanalyt. Chem.* 2010, **644**, 127.
[33] Q. S. Wang, J. H. Sun, C. H. Chen, X. M. Zhou *J. Therm. Anal. Chem.*, 2008, **92**, 563; M. Park, X. Zhang, M. Chung, G. B. Less and A. M. Sastry, *J. Power Sources*, 2010, **195**, 7904; P. Jeevan-Kumar, K. Jayanth-Babu, O. M. Hussain, C. M. Julien *Solid State Ionics* 2013, **19**, 421; M. Shui, S. Gao, J. Shu, W. D. Zheng, D. Xu, L. L. Chen, L. Feng, Y. L. Ren *Solid State Ionics* 2013, **19**, 47; W. C. West, J. Soler, M. C. Smart, B. V. Ratnakumar, S. Firdosy, V. Ravi, M. S. Anderson, J. Hrbacek, E. S. Lee and A. Manthiram *J. Electrochem. Soc.* 2011, **158**, A883-A889; M. Gozu, K. Swierczek, J. Molenda *J. Power Sources* 2009, **194**, 38; K. M. Shaju, G. V. S. Rao, B. V. R. Chowdari *J. Electrochem. Soc.* 2004, **151**, A1324.
[34] F. Nobili, S. Dsoke, F. Croce, R. Marassi, *Electrochimica Acta*, 2005, **50**, 2307.
[35] K. Nakamura, H. Ohno K. Okamura, Y. Michihiro, I. Nakabayashi, T. Kanashiro, *Solid State Ionics*, 2000, **135**, 143.